

Ab-Initio Surface Hopping and Multiphoton Ionisation Study of the Photodissociation Dynamics of CS₂

Darren Bellshaw,^a Daniel A. Horke,^{b,c} Adam D. Smith,^d Hannah M. Watts,^d Edward Jager,^d Emma Springate,^e Oliver Alexander,^e Cephise Cacho,^e Richard T. Chapman,^e, Adam Kirrander,^a and Russell S. Minns^d

^a*EaStCHEM, School of Chemistry, University of Edinburgh, David Brewster Road, Edinburgh EH9 3FJ, United Kingdom.*

^b*Center for Free-Electron Laser Science, DESY, Notkestrasse 85, 22607 Hamburg, Germany*

^c*The Hamburg Centre for Ultrafast Imaging, University of Hamburg, Luruper Chaussee 149, 22761 Hamburg, Germany*

^d*Chemistry, University of Southampton, Highfield, Southampton SO17 1BJ, UK*

^e*Central Laser Facility, STFC Rutherford Appleton Laboratory, Didcot, Oxfordshire OX11 0QX, UK*

Abstract

New *ab-initio* surface hopping simulations of the excited state dynamics of CS₂ including spin-orbit coupling are compared to new experimental measurements using a multiphoton ionisation probe in a photoelectron spectroscopy experiment. The calculations highlight the importance of the triplet states even in the very early time dynamics of the dissociation process and allow us to unravel the signatures in the experimental spectrum, linking the observed changes to both electronic and nuclear degrees of freedom within the molecule.

Keywords: Photodissociation, Photoelectron spectroscopy, Theoretical Chemistry, Non-adiabatic dynamics

1. Introduction

The dissociation dynamics of CS₂ following UV excitation have been a benchmark in chemical dynamics for many years, with numerous experimental studies in both the time and frequency domain, see for example [1, 2, 3, 4, 5, 6, 7, 8, 9, 10]. This lasting fascination with CS₂ can be traced

6 to the efficient dissociation, dictated by complex dynamics on multiple cou-
 7 pled electronic states. Despite intense experimental study, the fast dynamics
 8 and the high ionisation limits of intermediates and final products have lim-
 9 ited the experimental view to specific points along the full dissociation path,
 10 such that open questions remain even for this structurally simple molecule.
 11 The origin of the complexity derives from the near degeneracy of the op-
 12 tically bright ${}^1\text{B}_2({}^1\Sigma_u^+)$ state with multiple other electronic states at linear
 13 geometry, which leads to highly efficient population transfer and strongly
 14 coupled multistate dynamics. The mixing of the electronic states leads to
 15 dissociation and the formation of a ground state CS ($\text{X } {}^1\Sigma^+$) molecule in
 16 conjunction with atomic sulphur in either the spin forbidden ground state,
 17 ${}^3\text{P}$, or a spin allowed excited state, ${}^1\text{D}$. While the exact branching ratio has
 18 proven difficult to define accurately, the spin forbidden product is seen to
 19 dominate in most experimental studies [11, 2, 12], highlighting the impor-
 20 tance of spin-orbit coupling for an accurate description. Considering how well
 21 studied this molecule has been experimentally, calculations of the dynamics
 22 have been limited with, as far as we are aware, no simulations accounting for
 23 the spin-orbit coupling that drives the dominant dissociation process. In this
 24 work we combine *ab-initio* surface hopping simulations of the dissociation
 25 dynamics of CS_2 with new photoelectron spectroscopy measurements using
 26 a multiphoton probe to study the effect of spin-orbit coupling on the early
 27 time dynamics of the molecule.

28 Previous dynamics calculations have focused on the singlet state dynamics
 29 and the effect of non-adiabatic coupling on measured photoelectron angular
 30 distributions obtained following excitation at 201 nm and ionisation with 268
 31 nm [13]. These calculations provide a very good measure of the photoangular
 32 distribution, which they claim suggests that the lack of spin-orbit coupling
 33 in the model does not affect the calculated early time dynamics. It should be
 34 noted that the rather low energy probe used in the experiment means that
 35 only the singlet states could be ionised and that any effect of the triplet in
 36 the angular distributions would not be observable. The measurements and
 37 theory therefore do not take into account the population transfer between
 38 the initially excited singlet manifold and the accessible triplet states. This
 39 point is highlighted by recent time-resolved VUV photoelectron spectroscopy
 40 experiments by Spesyvtsev *et al.* [4] using a 20 fs 159 nm (7.8 eV) probe
 41 pulse. These experiments provide the most detailed maps of the excited
 42 state dynamics to date, and show large changes in electron kinetic energy as
 43 the molecule undergoes bending vibrations with an almost 3 eV shift in the

44 measured electron kinetic energy in 40 fs. The probed dynamics occur on the
 45 singlet surfaces and, as the molecule continues to vibrate, the population is
 46 transferred into lower lying electronic states which are outside the observation
 47 window provided even by their VUV probe.

48 2. Theory

49 2.1. Computational methods

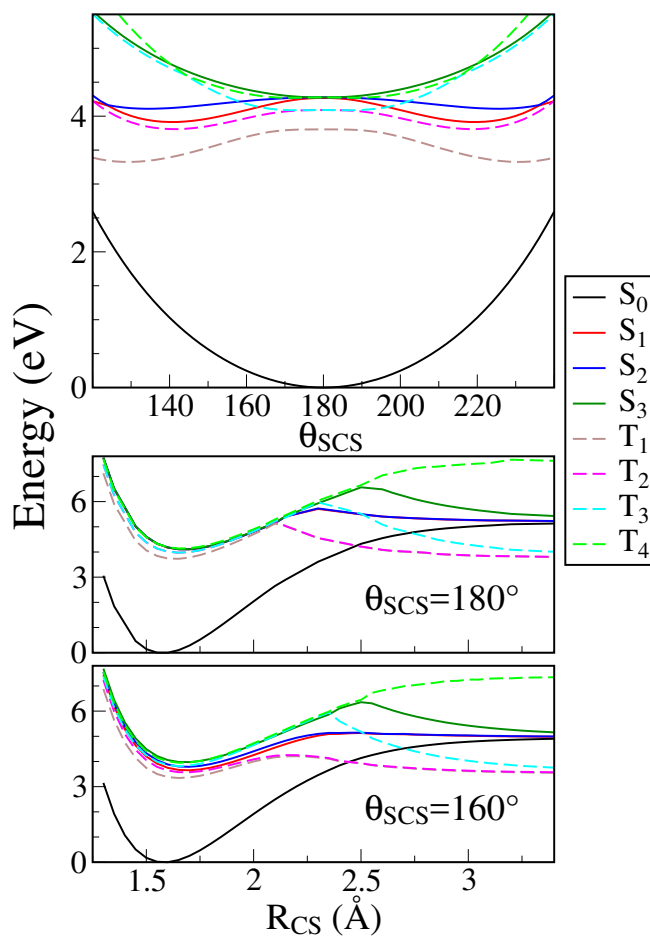


Figure 1: Bending θ_{SCS} (top), and radial asymmetric stretch R_{CS} for linear $\theta_{\text{SCS}}=180^\circ$ (middle) and bent $\theta_{\text{SCS}}=160^\circ$ (bottom), potential energy curves calculated at the SA8-CAS(16,12)/aug-cc-pvTZ level for the first four singlet and triplet states of CS₂. Remaining degrees of freedom are frozen at their equilibrium values.

50 *Ab-initio* electronic structure calculations were performed using the Mol-
 51 pro 2015.1 [14] suite of programs at the CAS(16,12)/aug-cc-pvTZ and aug-
 52 cc-pvQZ level of theory using the full valence (16,12) active space with bond-
 53 ing and antibonding σ and π molecular orbitals and sulfur atom lone pairs.
 54 Ground state geometry optimisation using CAS(16,12)/aug-cc-pvQZ resulted
 55 in $R_{\text{CS}}=1.569 \text{ \AA}$ and $\theta_{\text{SCS}}=0^\circ$. Angular and radial cuts through the singlet
 56 and triplet potential energy surfaces are shown in Fig. 1, and vertical excita-
 57 tion energies and oscillator strengths for the first four excited singlet states
 58 are given in Table 1. The potential energy curves in Fig. 1 are broadly in
 59 keeping with previous *ab-initio* calculations [15, 16, 17, 18, 19].

Table 1: Vertical excitation energies ($\Delta E = E(S_i) - E(S_0)$) and oscillator strengths from
 the ground state to the first four excited singlet states of CS_2 , calculated using SA5-
 CAS(16,12)-SCF/aug-cc-pvQZ with CASPT2 corrections to the energies. The excitation
 energies are calculated at the equilibrium geometry ($\theta_{\text{SCS}}=180^\circ$ and $R_{\text{CS}}=1.569 \text{ \AA}$), while
 oscillator strengths are calculated at $\theta_{\text{SCS}}=160^\circ$ since transition are very weak in the linear
 geometry.

| State | Energy (eV) | Oscillator strength |
|----------------|-------------|---------------------|
| S ₁ | 3.821 | 0 |
| S ₂ | 3.836 | 0.004282 |
| S ₃ | 3.836 | 0 |
| S ₄ | 6.430 | 0.000834 |

60 We simulate the dynamics of photoexcited CS_2 using the code SHARC
 61 [20, 21] interfaced with MOLPRO [14]. SHARC treats nuclear motion classi-
 62 cally, but nonadiabatic effects and spin-orbit coupling [22] are included using
 63 the fewest-switches surface-hopping approach [23]. The spin-orbit coupling
 64 is treated in the diabatic representation and has been shown to replicate
 65 branching dynamics in IBr when compared to full quantum dynamics simula-
 66 tions [22]. In contrast to previous singlet-only simulations [13], we propagate
 67 the dynamics on the four lowest singlet *and* triplet electronic states. To keep
 68 the simulations computationally feasible, we perform the electronic structure
 69 calculations at the SA8-CAS(8,6)-SCF/6-31G* level, which qualitatively re-
 70 produces the potential energy curves shown in Fig. 1. The differences to
 71 the CAS(16,12)/aug-cc-pvTZ level calculations are minor at small and large
 72 bond-lengths, but at intermediate distances the smaller active space gives rise
 73 to elevated barriers to dissociation, that lead to transient trapping of pop-
 74 ulation in the T2 state (see discussion in Section 2.2). Initial positions are

75 generated from a Wigner distribution based on the CAS(8,6)/6-31G* ground
 76 state vibrational frequencies and the oscillator strength of each geometry, and
 77 kinetic energy is assigned based on the required excitation energy and the
 78 experimental pump pulse energy. Following this protocol, 85% of trajectories
 79 begin in the $B\ ^1B_2$ state. A total of 369 trajectories are launched, of which
 80 197 reach 500 fs and 114 reach 1000 fs, using a time step of 0.5 fs. The reasons
 81 that some trajectories fail to reach 1000 fs are related to the electronic struc-
 82 ture calculations and include numerical problems such as excessive gradients
 83 in the CI or failure in convergence of the MCSCF calculations.

84 2.2. Computational results

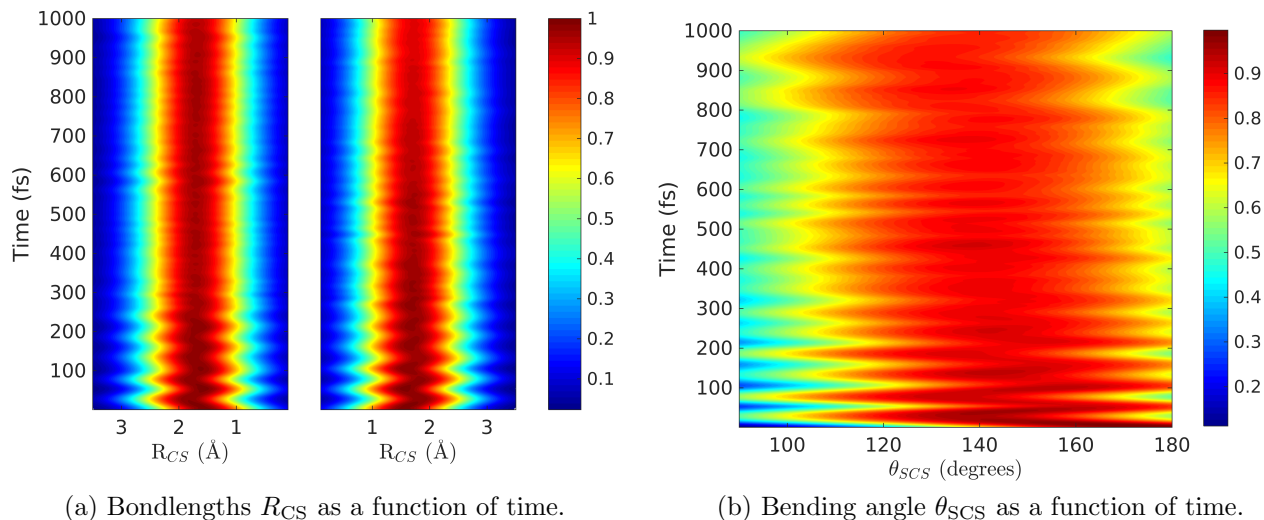


Figure 2: Probability density evolution of the CS_2 geometry in terms of the two bondlengths R_{CS} (Fig. 2a) and bending angle θ_{SCS} (Fig. 2b) from the simulations.

85 Excitation of CS_2 triggers bending and vibrational motion in the molecule,
 86 as can be seen in Fig. 2, which shows the probability density evolution of the
 87 molecular geometry as a function of the C-S bond-lengths, R_{CS} , and the
 88 bending angle, θ_{SCS} . During the first 100 fs the vibrations are dominated
 89 by the symmetric stretch, but at later times energy flows into the asym-
 90 metric stretch. The frequencies of vibrations are somewhat over-estimated
 91 compared to the experimental values, presumably due to slight differences
 92 in the *ab-initio* potential energy surfaces at the CAS(8,6) level. The total

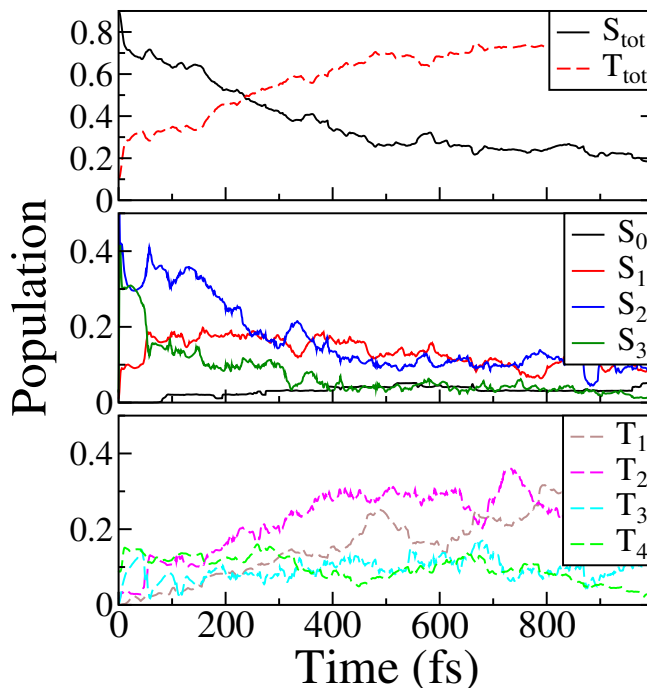


Figure 3: Time-dependent adiabatic state populations from simulation of CS₂ dynamics. The top panel shows the total singlet (excluding the S₀ ground state) and total triplet populations as a function of time. The middle panel shows the populations for each singlet state and the bottom panel the corresponding data for the triplet states.

fraction of dissociated molecules in the full set of 369 trajectories is 22%, which constitutes a lower bound since only about a quarter of the trajectories reach 1000 fs. Dissociation occurs predominantly in the triplet states, with 89% of the trajectories that dissociate occurring on the triplet surfaces. The lower degree of dissociation compared to the experiments can be traced to the topology of the potential energy surfaces at the level of *ab-initio* theory employed in the simulations, as discussed below.

The electronic state populations as a function of time are shown in Fig. 3. Initial excitation onto the S₂ ¹B₂(¹Σ_u⁺) state is followed by rapid decay onto the singlet S₃ and S₁ potentials, as well as a redistribution of population onto the manifold of triplet states via spin-orbit coupling. The nonadiabatic transfer of population between the singlet states correlates strongly with the bending motion of the molecule, with efficient transfer predominantly occurring close to the linear geometry where states are (near)-degenerate.

107 This gives rise to a periodic beating in both the individual singlet state
 108 populations and in the total singlet population. Over time there is a build-up
 109 of population in T_2 at $t > 400$ fs, and a subsequent rise of population in T_1 at
 110 around $t > 800$ fs, due to population transfer from T_2 to T_1 . The build-up in
 111 T_1 appears to be an artifact due to the SA8-CAS(8,6)-SCF/6-31G* *ab-initio*
 112 calculations, which increases the relative barrier height for dissociation on the
 113 T_1 and T_2 potentials by ≈ 1.5 eV (see Section 2.1), hindering dissociation
 114 and leading to the observed accumulation of population in T_2 . Consequently,
 115 it is reasonable to assume that the population trapped in T_2 in actual fact
 116 dissociates as observed in the experiment. Nevertheless, despite that the
 117 simulations underestimate the amount of $t < 1$ ps dissociation via the triplet
 118 states, the short-time $t < 400$ fs dynamics appears quite reliable.

119 **3. Experiment**

120 *3.1. Experimental methods*

121 The experiment has been described in detail previously [24]. Briefly, an
 122 amplified femtosecond laser system (Red Dragon, KM Labs) generates 30 fs
 123 pulses of 800 nm light, with a pulse energy of up to 10 mJ at a repetition
 124 rate of 1 kHz. The pump pulse is produced via fourth harmonic generation of
 125 the fundamental (800 nm) beam, generating photons at around 200 nm. The
 126 200 nm beam is produced using standard non-linear optics with sequential
 127 second, third and fourth harmonic generation in BBO giving a pulse energy
 128 of $\sim 1 \mu\text{J}$. The 400 nm probe is generated by second harmonic generation of
 129 the fundamental laser output, producing approximately $5 \mu\text{J}$ per pulse. The
 130 pump and probe beams are reflection focused in a near collinear geometry
 131 and cross at the centre of the interaction region of a velocity-map imaging
 132 (VMI) spectrometer [25], where they intersect the CS_2 molecular beam. The
 133 pump and probe beams are both linearly polarised in the plane of the VMI
 134 detector, perpendicular to the time-of-flight axis. The molecular beam is
 135 generated through the expansion of 5% CS_2 in He at 1 bar through a 1 kHz
 136 pulsed nozzle (Amsterdam cantilever [26]) with a $100 \mu\text{m}$ aperture. The re-
 137 sulting expansion passes through a 1 mm skimmer and enters the interaction
 138 region of the spectrometer through a hole in the centre of the repeller plate
 139 of the VMI spectrometer. The photoelectron spectra are obtained through
 140 polar onion-peeling of the background subtracted images [27]. Although the
 141 photoelectron angular distributions are obtained, they show no time depen-
 142 dence and as such are not discussed in the results section.

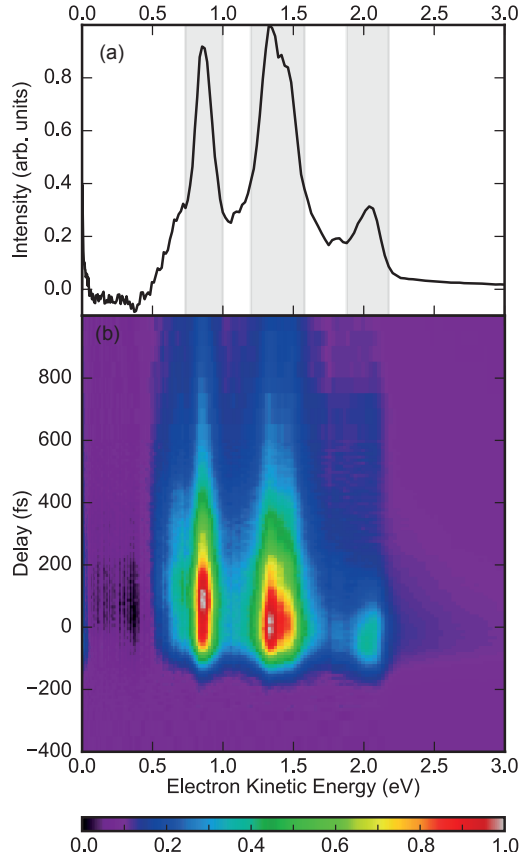


Figure 4: (a) Photoelectron spectrum obtained when the pump and probe pulses are temporally overlapped. The highlighted regions mark those used in the integrated plots shown in figure 5. (b) Photoelectron spectra as a function of pump-probe delay.

143 3.2. Experimental results

144 The 200 nm pump excites a vibrational wavepacket, predominantly in the
 145 S_2 1B_2 excited electronic state. The motion is then probed by non-resonant
 146 two-photon absorption at 400 nm. This provides a total energy of 12.5 eV,
 147 with the ionisation potential of CS_2 at 10.07 eV. The photoelectron signal
 148 obtained when the pump and probe pulse are overlapped in time is plotted
 149 in Fig. 4(a) with three main features around 2.1 eV, 1.4 eV and 0.9 eV
 150 electron kinetic energy. The spacing between the features is similar to that
 151 seen in previous single-photon ionisation measurements [1, 5]. The use of
 152 a multiphoton probe maintains a clean experimental measurement, without
 153 any probe-pump contributions at early times, while maximising the available

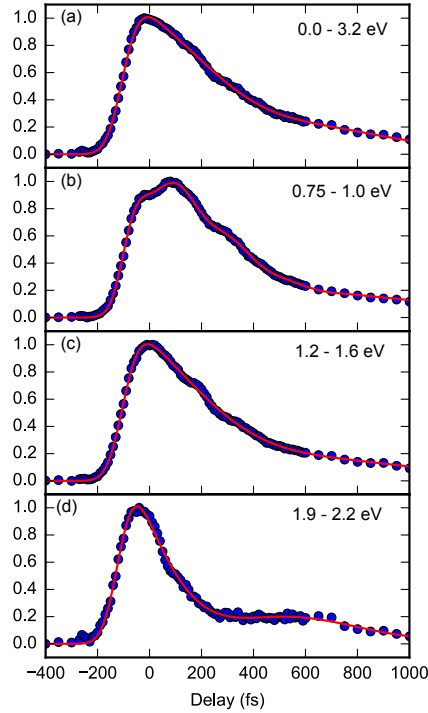


Figure 5: Total integrated photoelectron intensity (a) and intensity within the shaded areas shown in Fig. 4; 0.75 - 1.00 eV (b), 1.20 - 1.60 eV (c) and 1.90 - 2.20 eV (d). Solid lines represent fits to the data. (a,c,d) were fit with a single exponential decay, modulated by a single damped oscillator and convoluted with the instrument response function. However, a second oscillation with a period ~ 200 fs is clearly visible in the data. The data in (b) was fit with two damped oscillating components, which reproduce both observed oscillatory features well.

154 energy for ionisation, such that we can observe much of the initial excited
 155 state dynamics.

156 The time-dependence of the photoelectron spectrum is shown in Fig. 4(b).
 157 The three peaks in the spectrum have different appearance times, with those
 158 at lower electron kinetic energy appearing after those at higher electron ki-
 159 netic energy. The low-energy feature rises approximately 35 fs after the high-
 160 est energy feature at 2.1 eV. This maps the initial bending motion as seen
 161 in the calculated dynamics, Fig. 2b, and in previous measurements [4]. At
 162 longer delay times it is also clear that the centre of mass of the photoelectron
 163 spectrum shifts to lower electron kinetic energies, such that the lifetime of
 164 the measured photoelectron features is longer at lower electron kinetic ener-

gies. To obtain a clearer view of the changes observed at the various electron kinetic energies measured, we plot the integrated intensity over the features highlighted in Fig. 4(a) in Fig. 5. The difference in lifetime is apparent in the plots, as well as the appearance of clear oscillations in intensity that peak at times after time zero. The effect of the oscillations is most prominent in the feature centered around 0.9 eV, Fig. 5(b), which has a maximum intensity ~ 200 fs after excitation. None of the transients can therefore be fit to a simple exponential decay, but are modulated by at least one oscillating component. We therefore fit the transients to an exponential decay modulated by either one or two damped oscillations, convoluted with the instrument response function, corresponding to the laser pulse cross-correlation [28],

$$g \otimes \left(A_0 \exp\left(-\frac{t - t_0}{\tau}\right) \times \prod^n A_n \cos(\omega_n(t - t_0) + \delta_n) \right). \quad (1)$$

Here A_n represent intensity scaling parameters, t_0 the arrival time of the laser pulse, τ the exponential lifetime and ω and δ the angular frequency and phase of the oscillatory component. Fits are plotted as solid lines in Fig. 5. The highest energy feature, Fig. 5(d), provides the clearest data set and contains a single oscillation of period ~ 0.9 ps, 38 cm^{-1} , as has previously been experimentally observed [9, 10]. This corresponds to the beat between the ν_1 and ν_2 vibrational modes [8]. This is present in each of the other features in the spectrum, along with a second beat with a period around 200 fs. The effect of this oscillation is clearest in the trace presented in Fig. 5(b), however the mixing with the other oscillation and relatively low contrast makes assigning the absolute value of this oscillation difficult, leading to significant error margins. Nonetheless we extract an oscillation period of 220 fs, corresponding to 149 cm^{-1} , from this data. While this oscillation period does not fit with any of the known vibrational periods of the molecule, similar frequencies were also observed in a previous study [4] but were not discussed or assigned. The fits to the experimental data furthermore yield an increase in lifetime towards the lower electron kinetic energy regions. The $1/e$ lifetimes extracted are 401 fs, 452 fs and 457 fs for the peaks at 2.1 eV, 1.4 eV and 0.9 eV respectively.

4. Discussion

We now provide a comparison of the experimental measurements and the theoretical calculations. For both the calculations and experiment it is clear

198 that the triplet states play a large role in the dynamics from very early times.
 199 Significant population is transferred into the triplet states very rapidly with
 200 over 50% of the total population in the triplet states within 250 fs. The overall
 201 transfer of population approximately matches the decay rate measured in the
 202 experiment such that we are only sensitive to the singlet state population.
 203 As mentioned above the initial shift in the measured electron kinetic energy
 204 maps the initial bending motion of the molecule. As the pump-probe delay
 205 increases, the electron kinetic energy shifts towards lower values, such that
 206 we observe a longer lifetime for the lower electron kinetic energy regions in
 207 the spectrum in Fig. 5. To compare the measured signal to theory, in Fig.
 208 6 we plot the singlet state component of Fig. 2. Initial excitation leads to a
 209 wavepacket that oscillates between linear geometries and an angle of $\sim 110^\circ$.
 210 With increasing pump-probe delay, the range of angles explored narrows and
 211 moves away from the linear geometries associated with the spectral feature
 212 at the highest electron kinetic energy. Within the current experiment we do
 213 not have the time resolution to fully resolve the bending motion, but we do
 214 observe the effect of the narrowing and shifting of the angles explored by the
 215 molecule as a corresponding narrowing and shifting to lower electron kinetic
 216 energies in the photoelectron spectrum.

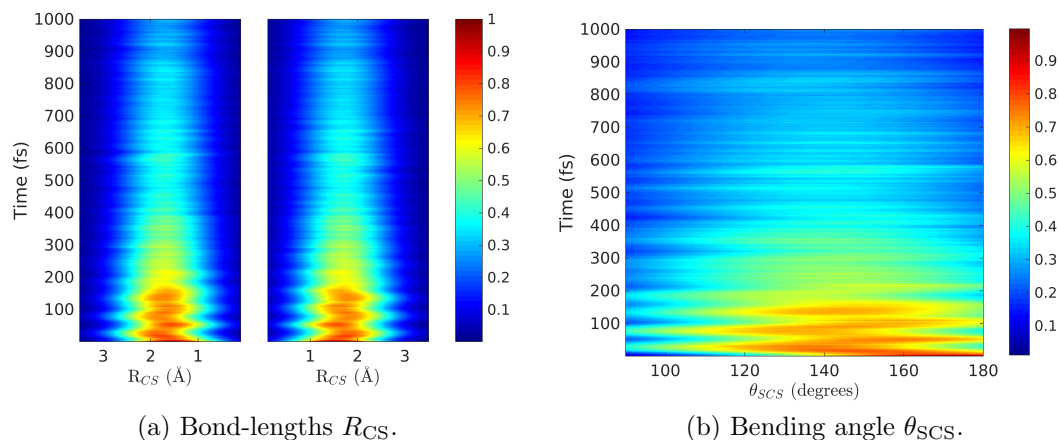


Figure 6: Probability density evolution of the CS₂ geometry in terms of the two bond-lengths R_{CS} and bending angle θ_{SCS} in the singlet states only. The intensity bar shows the total population with the decreasing intensity showing the transfer of population into the triplet states.

217 As mentioned above, the short time period oscillation seen both in the

total photoelectron count rate and, in individual regions of the photoelectron spectrum (Fig. 5), do not match any vibrational periods within the molecule. The simulations also show no obvious changes in the molecular structure that appear to provide an explanation for the oscillations. The calculations do show periodic changes in total singlet excited state population that correlate with the observed changes the photoelectron yield. We therefore tentatively assign the oscillations in the experimental spectrum to changes in the total singlet state population.

5. Summary

We have performed a combined theory and experiment study of the excited state dynamics of CS_2 . The ab-initio surface-hopping simulations highlight the importance of the triplet states in the early time dynamics with significant population transfer predicted, and observed in the complementary time-resolved photoelectron spectroscopy measurements. The combined work demonstrates that one can now do on-the-fly dynamics including spin-orbit coupling. The accuracy of the calculation is such that we are able to directly compare the results of the calculation with experiment and explain the shifting and narrowing of the photoelectron spectrum in terms of the bending motion and angles explored by the vibrational wavepacket, while oscillation in the measured photoelectron count rate are explained by the complex coupling of the electronic states that leads to rapid population transfer between manifolds of multiple singlet and triplet excited states. Measuring the longer term dynamics in the triplet states is an experimental challenge. Recent experiments by the Suzuki group using a 7.8 eV probe showed no clear contributions from the triplet states suggesting ionisation requires higher energies.[4] This is presumably due to the ionisation propensity of the triplet states being into electronically excited ion states. Measurements of the dynamics outside of the initially excited singlet states will therefore require measurement using a significantly higher photon energy such as that available from a high harmonic generation source. Such experiments are currently ongoing and will be the subject of a future publication.

Acknowledgments

All authors thank the STFC for access to the Artemis facility (app. number 13220015). RSM thanks the Royal Society for a University Research

Fellowship (UF100047) and the Leverhulme trust for research support and
 for ADS’s studentship (RPG-2013-365). HMW thanks the Central Laser Fa-
 cility and Chemistry at the University of Southampton for a studentship.
 EJ thanks Chemistry at the University of Southampton for a studentship.
 We also acknowledge funding from the EC’s Seventh Framework Programme
 (LASERLAB-EUROPE, grant agreement n° 228334). We thank Phil Rice for
 technical assistance. This work has been supported by the excellence cluster
 ”The Hamburg Center for Ultrafast Imaging – Structure, Dynamics and Con-
 trol of Matter at the Atomic Scale” of the Deutsche Forschungsgemeinschaft
 (CUI, DFG-EXC1074). D.A.H. was supported by the European Research
 Council through the Consolidator Grant Küpper-614507-COMOTION. AK
 acknowledges funding from the European Union (FP7-PEOPLE-2013-CIG-
 NEWLIGHT) and the Leverhulme Trust (RPG-2013-365), and DB acknowl-
 edges a PhD studentship from the University of Edinburgh. The computa-
 tional work reported used the ARCHER UK National Supercomputing Ser-
 vice (<http://www.archer.ac.uk>) and the Edinburgh Compute and Data Facil-
 ity (ECDF) (<http://www.ecdf.ed.ac.uk>). DB thanks Sebastian Mai (Wien)
 for helpful discussions.

- [1] D. Townsend, H. Satzger, T. Ejdrup, A. M. D. Lee, H. Stapelfeldt,
 A. Stolow, $^1\text{b}_2$ excited state decay dynamics in cs_2 , J. Chem. Phys. 125
 (2006) 234302.
- [2] T. N. Kitsopoulos, C. R. Gebhardt, T. P. Rakitzis, Photodissociation
 study of cs_2 at 193 nm using slice imaging, J. Chem. Phys. 115 (2001)
 9727.
- [3] M. Brouard, E. K. Campbell, R. Cireasa, A. J. Johnsen, W.-H. Yuen,
 The ultraviolet photodissociation of cs_2 : The $s(^1\text{d}_2)$ channel, J. Chem.
 Phys. 136 (2012) 044310.
- [4] R. Spesyvtsev, T. Horio, Y.-I. Suzuki, T. Suzuki, Observation of the
 wavepacket dynamics on the $^1\text{b}_2(^1\sigma_u^+)$ state of cs_2 by sub-20 fs photo-
 electron imaging using 159 nm probe pulses, The Journal of Chemical
 Physics 142 (2015).
- [5] C. Z. Bisgaard, O. J. Clarkin, G. Wu, A. M. D. Lee, O. Gener, C. C.
 Hayden, A. Stolow, Time-resolved molecular frame dynamics of fixed-
 in-space cs_2 molecules, Science 323 (2009) 1464.

- [6] T. Horio, R. Spesyvtsev, T. Suzuki, Simultaneous generation of sub-20 fs deep and vacuum ultraviolet pulses in a single filamentation cell and application to time-resolved photoelectron imaging, *Opt. Express* 21 (2013) 22423.
- [7] T. Horio, R. Spesyvtsev, T. Suzuki, Generation of sub-17fs vacuum ultraviolet pulses at 133nm using cascaded four-wave mixing through filamentation in ne, *Opt. Lett.* 39 (2014) 6021.
- [8] R. J. Hemley, D. G. Leopold, J. L. Roebber, V. Vaida, The direct ultraviolet absorption spectrum of the $^1\sigma_g^+ \rightarrow ^1b_2(^1\sigma_u^+)$ transition of jetcooled cs₂, *J. Chem. Phys.* 79 (1983) 5219.
- [9] P. Farmanara, V. Stert, W. Radloff, Ultrafast predissociation and coherent phenomena in CS₂ excited by femtosecond laser pulses at 194–207 nm, *The Journal of Chemical Physics* 111 (1999) 5338–5343.
- [10] P. Hockett, C. Z. Bisgaard, O. J. Clarkin, A. Stolow, Time-resolved imaging of purely valence-electron dynamics during a chemical reaction, *Nat Phys* 7 (2011) 612–615.
- [11] I. M. Waller, J. W. Hepburn, Photofragment spectroscopy of cs₂ at 193 nm: Direct resolution of singlet and triplet channels, *J. Chem. Phys.* 87 (1987) 3261.
- [12] D. Xu, J. Huang, W. M. Jackson, Reinvestigation of cs₂ dissociation at 193 nm by means of product state-selective vacuum ultraviolet laser ionization and velocity imaging, *J. Chem. Phys.* 120 (2004) 3051.
- [13] K. Wang, V. McKoy, P. Hockett, M. S. Schuurman, Time-Resolved Photoelectron Spectra of CS₂: Dynamics at Conical Intersections, *Phys. Rev. Lett.* 112 (2014) 113007.
- [14] H.-J. Werner, P. J. Knowles, G. Knizia, F. R. Manby, M. Schütz, et al., Molpro, version 2015.1, a package of ab initio programs, 2015. See.
- [15] D. Tseng, R. Poshusta, Ab initio potential energy curves for low-lying states of carbon disulfide, *The Journal of chemical physics* 100 (1994) 7481–7486.

- [16] Q. Zhang, P. H. Vaccaro, Ab initio studies of electronically excited carbon disulfide, *The Journal of Physical Chemistry* 99 (1995) 1799–1813.
- [17] S. T. Brown, T. J. Van Huis, B. C. Hoffman, H. F. Schaefer III, Excited electronic states of carbon disulphide, *Molecular Physics* 96 (1999) 693–704.
- [18] K. B. Wiberg, Y.-g. Wang, A. E. de Oliveira, S. A. Perera, P. H. Vaccaro, Comparison of cis-and eom-ccsd-calculated adiabatic excited-state structures. changes in charge density on going to adiabatic excited states, *The Journal of Physical Chemistry A* 109 (2005) 466–477.
- [19] A. Mank, C. Starrs, M. Jago, J. Hepburn, A detailed study of the predissociation dynamics of the 1b2 ($1\sigma + u$) state of cs₂, *The Journal of chemical physics* 104 (1996) 3609–3619.
- [20] S. Mai, M. Richter, M. Ruckebauer, M. Oppel, P. Marquetand, L. González, Sharc: Surface hopping including arbitrary couplings program package for non-adiabatic dynamics, sharc-md.org, 2014.
- [21] M. Richter, P. Marquetand, J. González-Vázquez, I. Sola, L. González, SHARC: ab initio molecular dynamics with surface hopping in the adiabatic representation including arbitrary couplings, *J. Chem. Theory Comput.* 7 (2011) 1253–1258.
- [22] S. Mai, P. Marquetand, L. González, A general method to describe intersystem crossing dynamics in trajectory surface hopping, *Int. J. Quantum Chem.* 115 (2015) 1215–1231.
- [23] J. C. Tully, Molecular dynamics with electronic transitions, *The Journal of Chemical Physics* 93 (1990) 1061–1071.
- [24] A. D. Smith, H. M. Watts, E. Jager, D. A. Horke, E. Springate, O. Alexander, C. Cacho, R. T. Chapman, R. S. Minns, Resonant multiphoton ionisation probe of the photodissociation dynamics of ammonia, *Phys. Chem. Chem. Phys.* 18 (2016) 28150–28156.
- [25] A. Eppink, D. Parker, Velocity map imaging of ions and electrons using electrostatic lenses: Application in photoelectron and photofragment ion

- 347 imaging of molecular oxygen, Review of Scientific Instruments 68 (1997)
348 3477–3484.
- 349 [26] D. Irimia, D. Dobrikov, R. Kortekaas, H. Voet, D. A. van den Ende,
350 W. A. Groen, M. H. M. Janssen, A short pulse (7 μ s FWHM) and
351 high repetition rate (dc-5kHz) cantilever piezovalve for pulsed atomic
352 and molecular beams, Review of Scientific Instruments 80 (2009) 113303.
- 353 [27] G. M. Roberts, J. L. Nixon, J. Lecointre, E. Wrede, J. R. R. Verlet, To-
354 ward real-time charged-particle image reconstruction using polar onion-
355 peeling, Review of Scientific Instruments 80 (2009) 053104.
- 356 [28] D. Hanggi, P. W. Carr, Errors in exponentially modified Gaussian equa-
357 tions in the literature, Analytical Chemistry 57 (1985) 2394–2395.